The 2010 IEEE/RSJ International Conference on
Intelligent Robots and Systems
October 18-22, 2010, Taipei, Taiwan

Realistic Visual and Haptic Feedback Simulator for Real-time Cell Indentation

Hamid Ladjal, Jean-Luc Hanus, Anand Pillarisetti, Carol Keefer, Antoine Ferreira and Jaydev P. Desai

Abstract—**Comprehensive and training simulators that provide realistic visual and haptic feedback during cell indentation tasks are currently investigated. Complex cell geometry inherent to biological cells and intricate mechanical properties drive the need for precise mechanical and numerical modeling to assure accurate cell deformation and force calculations. Advances in alternative finite element formulation, such as mass-tensor approach, have reached the state where they are applicable to model soft cell deformation in real time. The geometrical characteristics and the mechanical properties for different cells are determined with AFM indentation. A real-time, haptics-enabled simulator for cell centered indentation has been developed which utilizes the atomic force microscopy data (mechanical and geometrical properties of embryonic stem cells (mESC)) to accurately replicate the indentation task and predict the cell deformation during indentation in real-time. This tool can be used as a mechanical marker to characterize the biological state of the cell. The operator is able to feel in real-time the change in the stiffness during cell deformation between fixed and live cells. A comparison study with finite element simulations using a commercial software and the experimental data demonstrate the effectiveness of the proposed physically-based model.**

I. Introduction

Mechanical manipulation and characterization of biological cells is currently one of the promising research areas in the field of medical robotics applied to cellular level interactions. The mechanical properties such as elasticity, membrane tension, cell shape, and adhesion strength may play an important role in the cell fate and differentiation [1]. Embryonic stem cells (mESCs) can give rise to every cell type in the body unlike adult stem cells and thus have huge therapeutic potential. Stem cell based systems offer a very promising and innovative alternative for obtaining large number of cells for early efficacy and higher toxicity screening. Stem cell technology provides a new tool for drug development and an insight to better understand mammalian gene function. The mechanical properties of biological cells have been studied with different techniques [2], the most popular are optical tweezers [3], magnetic beads [4], and micropipette aspiration [5]. AFM has been widely used in the study of micro- and nanostructures including living cells [6]. Modern AFM techniques allow solving a number of problems of cell biomechanics by simultaneous evaluation of the local mechanical properties and the topography of the living cells, at a high spatial resolution and force sensitivity [7]. In these experiments AFM cantilever serves as a microindenter to probe the cell, and further analysis of force-indentation data yields the local Young's modulus. In addition, AFM indentation technique can be used to characterize the viscoelastic behavior of the cell cytoskeleton [8], including viscosity [9], loss and storage moduli [10], and stress relaxation times. AFM-based indentation techniques with force feedback have been applied here to characterize single-cell mouse embryonic stem cells (mESCs) [11]. We developed finite element models that include the topological information of adherent stem cells (shape and dimensions) and AFM tips (conical, spherical), and biological structure (cells models with cytoplasm layers, cytoskeletons and nucleus) [12]. The proposed indentation tests use microsphere-modified AFM probes in order to estimate global elastic modulus for the cell to reflect the true global response of a mESCs [12]. The paper consists of five sections. In Section II, we present the bio-mechanical finite element model in real-time indentation. In Section III, we present the methodology of the virtual environment system for cell indentation. In Section IV, we present the experimental setup using the force microscopy. In Section V, we make a comparative study between the physics-based model and experimental data. In Section VI, we present our real-time cell indentation simulator using a spherical tip. Finally, we give some concluding remarks and the directions for future work.

H. Ladjal, J-L Hanus and A. Ferreira are with Institut PRISME, ENSI of Bourges 88, Boulevard Lahitolle, France antoine.ferreira@ensi-bourges.fr

A. Pillarisetti, J.P. Desai are with the Department of Mechanical Engineering, University of Maryland, College Park, MD, USA jaydev@umd.edu

C. Keefer is with the Department of Animal and Avian Sciences, University of Maryland, College Park, MD, USA

II. Physically Based Modeling of Deformable Objects for Cell Nanoindentation Simulation

In this section we present different steps for the linear elastic mass-tensor model introduced by [13] and extended by the authors in [14]. In our work, the cell is modeled by the volume object discretized into a conformal tetrahedral mesh as defined by finite element theory. Using classical notations, inside each tetrahedron T^k, the displacement field, defined by a linear interpolation $\left[\mathbf{N^k}\right]$ of the nodal displacement vector $\left\{\mathbf{u^k}\right\}$ of the four vertices of tetrahedron, is written as follows:

$$\left\{\mathbf{U}(\mathbf{x})^{\mathbf{k}}\right\} = \left[\mathbf{N^k}(\mathbf{x})\right] \quad \left\{\mathbf{u^k}\right\} \tag{1}$$

For a linear elastic material, the relation between the Cauchy stress tensor and the linearized strain tensor is written with Lame's coefficient in condensed vector notation as :

$$\left\{\boldsymbol{\sigma}\right\} = \lambda \left(\left\{\boldsymbol{\varepsilon}\right\}_1 + \left\{\boldsymbol{\varepsilon}\right\}_2 + \left\{\boldsymbol{\varepsilon}\right\}_3 \right) \left[\mathbf{I}\right] + 2\,\mu \left\{\boldsymbol{\varepsilon}\right\} \tag{2}$$

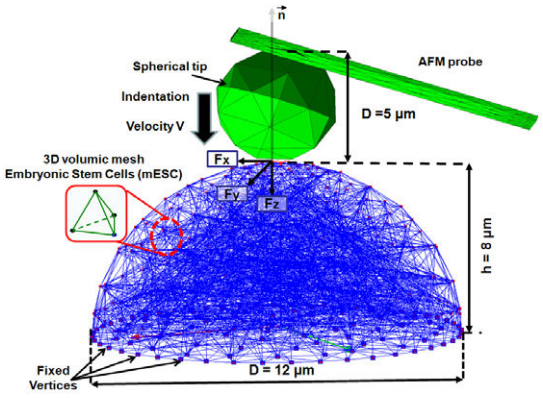

Fig. 1. Representation of the 3D mESC mesh using P1 tetrahedral finite elements.

where $\left[\mathbf{I}\right]$ is the identity matrix.
The principle of virtual work applied to a single tetrahadron T^k leads to the elementary stiffness matrix $\left[\mathbf{K^k}\right]$ such that the elementary nodal force vector acting on a tetrahedron is:

$$\left\{\mathbf{f^k}\right\} = \left[\mathbf{K^k}\right] \left\{\mathbf{u^k}\right\} \tag{3}$$

This stiffness matrix is composed of a plurality of elementary submatrices each connecting the elementary force acting on the node, i, to the displacement of the node, j:

$$\left[\mathbf{K_{ij}^k}\right] = \frac{1}{36\,V^k}\left(\lambda \left\{\mathbf{m_i}\right\}\left\{\mathbf{m_j}\right\}^T + \mu\left\{\mathbf{m_j}\right\}\left\{\mathbf{m_i}\right\}^T + \mu\left\{\mathbf{m_i}\right\}^T\left\{\mathbf{m_j}\right\}\left[\mathbf{I}\right]\right) \tag{4}$$

where $\left\{\mathbf{m}\right\}$ are unit outward-pointing normals to triangular faces and V^k is the volume of the tetrahedron T^k. Taking into account the contribution of all adjacent tetrahedra, the global internal force acting on a node l can be expressed as follows:

$$\left\{\mathbf{F_{int}^l}\right\} = \sum_{k\in\mathcal{V}_l}\left(\sum_{j=1}^{4}\left[\mathbf{K_{ij}^k}\right]\left\{\mathbf{u_j}\right\}\right) \tag{5}$$

where $\mathcal{V}_l$ is the neighborhood of vertex l (i.e. the tetrahedra containing node l).
The tensors $\left[\mathbf{K_{ij}^k}\right]$, depending on the rest geometry and Lame's coefficients, are constant. They can be pre-computed in an off-line phase. It's the essential advantage of the mass-tensor approach which makes it useful for real-time application.

A. Cell modeling using finite element model

In our work, the mESC is meshed with 3D first-order tetrahedral elements as shown in Fig.1. The mesh that has been used for the following simulations is constituted by a non regular volume mesh composed of 835 vertices and 2456 tetrahedra where all vertices are free to move except the ones in contact with the petridish which are fixed.

B. Dynamic Model

The equation of motion of a vertex, l, of the cell mesh can be written:

$$M^l\left\{\ddot{\mathbf{u}}_l\right\} + \gamma^l\left\{\dot{\mathbf{u}}_l\right\} + \sum_{k\in\mathcal{V}_l}\left(\sum_{j=1}^{4}\left[\mathbf{K_{ij}^k}\right]\left\{\mathbf{u_j}\right\}\right) = \left\{\mathbf{F_{ext}^l}\right\} \tag{6}$$

where M^l and γ^l are respectively the mass and damping coefficients of each vertex.
To solve the dynamic system, we tested different integration schemes (implicit and explicit) taking into account the tradeoff between real-time simulation and haptic stability requirements. We choose the explicit centered finite-difference scheme defined by:

$$\begin{cases} u(t+h) = u(t) + \dot{u}(t)\,h + \frac{1}{2}\ddot{u}(t)\,h^2 + O(h^3) \\ \dot{u}(t+h) = \dot{u}(t) + \frac{1}{2}\ddot{u}(t)\,h + \frac{1}{2}\ddot{u}(t+h)\,h + O(h^3) \end{cases} \tag{7}$$

where h is the temporal integration step size chosen to satisfy the Courant-Friedrich-Lewy condition.

III. A VIRTUAL ENVIRONMENT SYSTEM FOR CELL INDENTATION

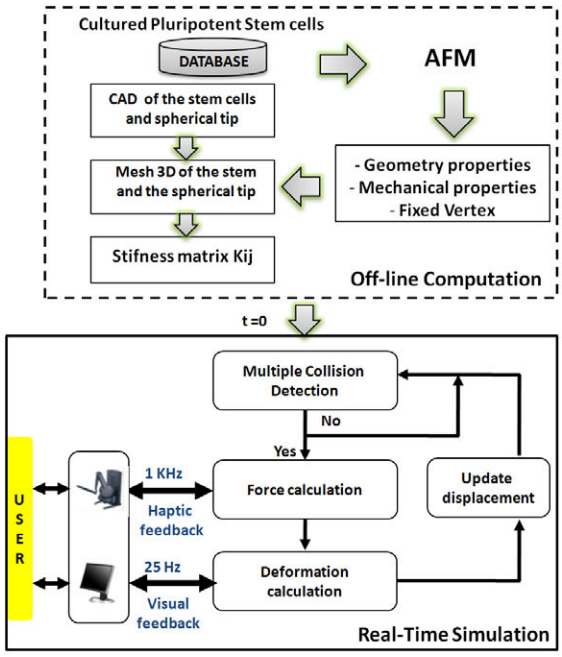

Fig. 2. Computational architecture for simulating force-reflecting deformable cell indentation in virtual environment. The figure shows the two simulation phases used for the real-time indentation of the cell: (i) off-line pre-calculations of stiffness matrices and (ii) simulation of visual and haptic interaction.

Fig.2 shows the architecture of the real-time virtual reality based cell indentation simulator. A significant difficulty of using the finite element technique for real-time simulation is that it is computationally costly. These mesh-based schemes also require an expensive numerical integration operation for the computation of the system stiffness matrices. For

this reason we adopted an off-line computation of entries of stiffness matrix for each triangular element and a real-time visual and haptic interaction for indentation simulation.

A. Off-line computation

All the operations costly in time are realized during this step. Using atomic force microscopy (AFM) image analysis (ImagePro software from AFM Asylum), the mechanical and geometrical properties of the cell structure are determined through AFM indentation experiments and validated using analytical Hertz contact modeling. The off-line calculation of all tensors K_{ij} allows pre-calculation stiffness values for a wide range of cell deformations.

B. Real-time Indentation

During the indentation task, the contact between the tip and the cell must occur at a special set of points (nodal points).

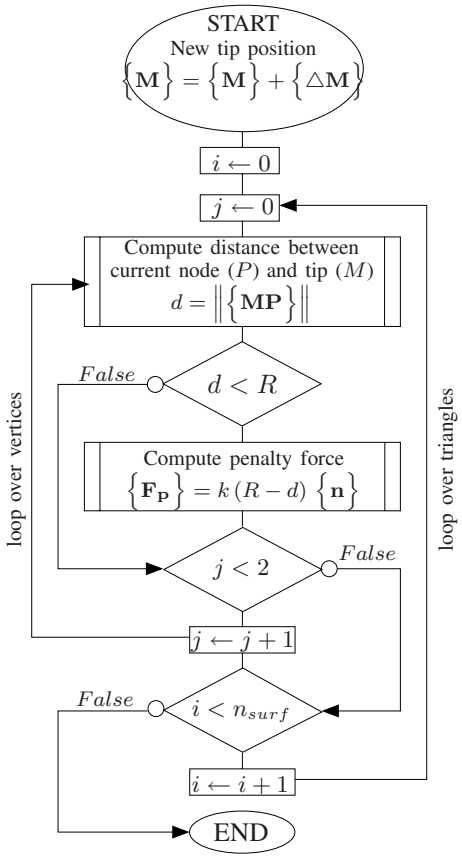

Fig. 3. Multi collision detection flowchart between a spherical tip and a stem cell: M represents the position of the center of the spherical tip and R its radius, $\{\triangle M\}$ represents the step of the imposed displacement, d is the computed distance between the center of the tip and a node of the external cell surface, F_{rep} represents the repulsive force and $\{n\}$ the outward-pointing normal

1) Collision Detection: The collision detection is the first step to carry out realistic interactions. However, locating the contact primitive (e.g. facets) between two objects may be computationally expensive, especially if the objects are composed of a large number of polygons. In general, to determine a contact between two virtual objects we compute the distance between them. If this distance is negative then the objects are in contact. The cantilever tip in virtual environment can be modeled as a complex 3D object, composed of numerous surfaces, edges and vertices but it constitutes a challenging task. For the purposes of detecting collisions, we used a point-based representation of the cantilever tip as a simple spherical object and employed a simple sphere-points intersection algorithm with local search technique (See Fig. 3). It calculates the distance between the center of the spherical tip and the nodes of the cell surface (see Fig. 4).

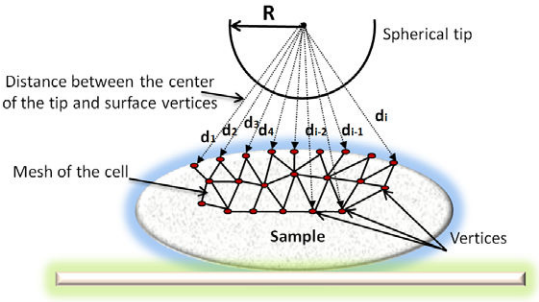

Fig. 4. Scheme illustrating the multiple collision detection algorithm using a simple sphere-points intersection problem: the distance between the center of the spherical tip and the nodes of the cell surface is calculated in real-time.

2) Penalty based models: In an interaction model, a collision between two objects may generate local and global deformations of the colliding objects. In our simulations we used the penalty based models. This model considers the reactive force that first reduces the relative speed of the two objects and finally repulses them from each other, as proportional to the deformation. Thus the reactive force is a function of the local interpenetration depth δ. The normal repulsive force F_{rep}, can be written:

$$\left\{\mathbf{F_{rep}}\right\} = \lambda\,\delta\,\left\{\mathbf{n}\right\} \tag{8}$$

where λ is the penalty of the interpenetration and $\left\{\mathbf{n}\right\}$ the outward-pointing normal.

3) Virtual coupling for stability of the haptic rendering: The internal operating loop of the haptic interface requires an update frequency neighboring of $1KHz$. However, the finite element model update frequency between the 25 and $30Hz$. This frequency difference does not ensure the coherence between both systems leading to instabilities of the user haptic rendering. We adopted the solution to use a virtual coupling model defined in [19].

IV. Experimental Setup

A. Description

The experimental tests of the cells indentations were performed using an atomic force microscope (Model: MFP-3D-BIO, Asylum Research, Santa Barbara, CA). The atomic force microscope (AFM) is integrated with a top view

module and mounted on an active vibration isolation table manufactured by Herzan (Laguna Hills, CA) as shown in Fig. 5. The top view module enables viewing of cells and easy alignment of the laser beam on the AFM cantilever. The XY stage (manual) allows the user to position the cell beneath the cantilever tip of AFM. The entire AFM set up is enclosed in an acoustic isolation chamber to prevent acoustic noise from interfering with the AFM measurements. The x- and y-axes range of the scan head is 90μm. The z-axis scan range is 40μm. The deflection of the cantilever is detected

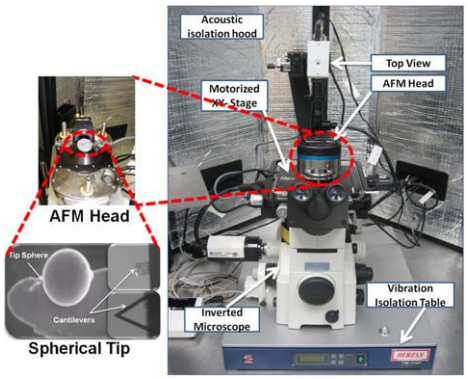

Fig. 5. Atomic Force Microscopy: The experimental set up for indentation studies and spherical geometrical Tip used for(mESC): The cantilevers attached with a spherical probe ($5\mu m$ in diameter), the silicon nitride cantilever (Novascan Technologies, Inc.)

by a photodiode when the tip comes in contact with the cell. When the tip of the cantilever is in contact with the cell, the initial cantilever deflection, (d_0), and initial cantilever movement in (z) direction (z_0) are stored. As the cantilever moves in the z direction and deforms the cell, the final cantilever deflection, (d_1), and the cantilever movement, (z_1) are obtained [17]. The geometry and spring constant of the cantilever are calibrated in the same way for the live and fixed cells. In the following experiments, we employed two types of cantilevers attached with a spherical probe (5 μm in diameter):

- Silicon nitride cantilever with a spring constant of 0.06 N/m (Novascan Technologies, Inc., Ames,IA) for live cells.
- Silicon cantilever with a spring constant of 1.75 N/m (Novascan Technologies, Inc) for fixed cells.

V. Mouse Embryonic Stem Cells Characterization

A. Geometry of the cell and cantilever interaction with the surface

The cells were 10 and 15 μm in diameter using the cantilever tip to measure the interaction force between the cell and the tip. The geometric modeling of the cell requires the determination of the height, adhesion surface and cell's contour (see Fig.6). The mESC height was calculated from the force-displacement curve obtained on: hard surface and on mESC surface. First, initial height h_0 is measured by bringing the AFM tip in contact with the hard surface near mESC and then the second height h_1 by bringing the AFM tip on mESC surface. The mESC height is the difference between $h = h_0 - h_1$. Second, to determine mESC shape, AFM imaging experiments are carried out in order to determine mESC's contour and diameter using the image processing techniques [15]. From Fig.6 we selected mESC

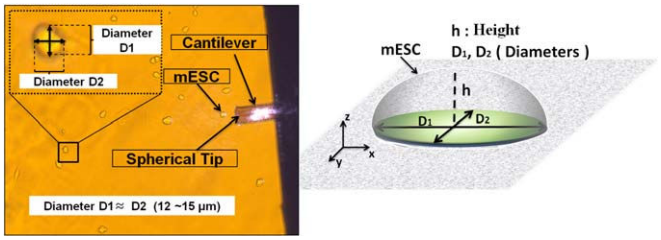

Fig. 6. How to determine the diameter of the stem cell through image analysis (ImagePro software from Asylum).

shapes with circular adhesion surfaces. As illustration, the left corner inset shows a typical circular mESC where D_1 and D_2 stands for the horizontal cells diameters ($D_1 \simeq D_2$ close to $12\mu m$).

B. Comparison between experimental data and analytical models

To estimate the mechanical properties of biological cells using the AFM, various analytical models can be used to identify Young's modulus of mESC in live as well as fixed cells. We performed single indentation studies with a spher-

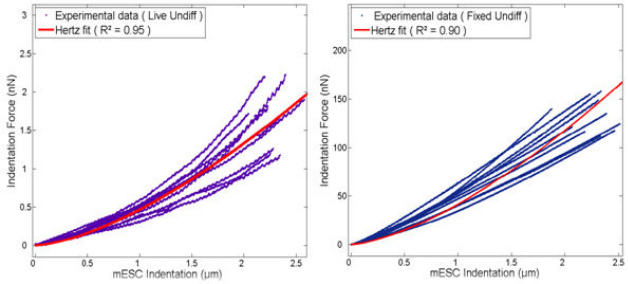

Fig. 7. Force versus indentation for live and fixed mESC.

ical tip on mESC. The main goal is to determine whether it appropriately predicts the force-indentation relationship of mESC [15]. The figure Fig.7 shows the force versus cell indentation for live and fixed undiff mESC using the Hertz model. The relationship between the indentation δ, and the loading force F is given by:

$$F = \frac{4}{3} E^* R^{\frac{1}{2}} \delta^{\frac{3}{2}} \tag{9}$$

where E^*, R are the combined modulus and the relative curvature of the tip and the cell respectively

$$\frac{1}{E^*} = \frac{1-\nu_1^2}{E_1} + \frac{1-\nu_2^2}{E_2} \tag{10}$$

TABLE I
MECHANICAL AND GEOMETRICAL PROPERTIES USED IN THE HAPTICS-ENABLED SIMULATOR

	Live mESC	Fixed mESC
Young modulus (KPa)	0.169	26.7
Poisson coefficient	0.49	0.49
Diameter(μm)	$\simeq 12$	$\simeq 12$
Height (μm)	8	8

$$\frac{1}{R} = \frac{1}{R_1} + \frac{1}{R_2} \tag{11}$$

where (E_1, ν_1, R_1) and (E_2, ν_2, R_2) represent the elastic

Fig. 8. Real-time indentation simulator using the Omni haptic interface.

modulus, Poisson's ratio, and the radius of the cell and spherical indenter respectively. The elastic modulus of the silicon nitride cantilever and silicon cantilever were 222.22 GPa and 168.17 GPa used for the live and fixed cells respectively. The elastic modulus of the cells is in range of KPa. Hence, our assumption that the tip used for probing is infinitely stiff compared to the cell and Hertz contact model is valid. Thus, Eq. 9 can be rewritten as:

$$F = \frac{4E_1}{3(1-\nu_1^2)} R_1^{\frac{1}{2}} \delta^{\frac{3}{2}} \tag{12}$$

VI. FINITE ELEMENT MODEL (FEM) SIMULATION OF CELL INDENTATION

The Fig.8 presents a photo of visual and haptic user interface setup. To test the accuracy and reliability of the proposed user interface system with haptics enabled simulation, a set of experiments is designed using the setup given in Section 2. The geometrical dimensions of the cell are determined through AFM image processing and force curve deflection (diameter and height) and the mechanical properties through AFM indentation studies thanks to the use of an analytical Hertz contact model.

In order to demonstrate the validity of our finite element indentation model in real-time, we compared the simulation indentation using the physically-based FEM model to the incremental data provided by AFM indentation tool and to the response simulated with a commercial FE software. The figures (Fig.9, Fig.10) present the nonlinear relationship between the penetration distance (indentation) and the reaction force for live and fixed undiff cells. The finite element simulations using the commercial software show good

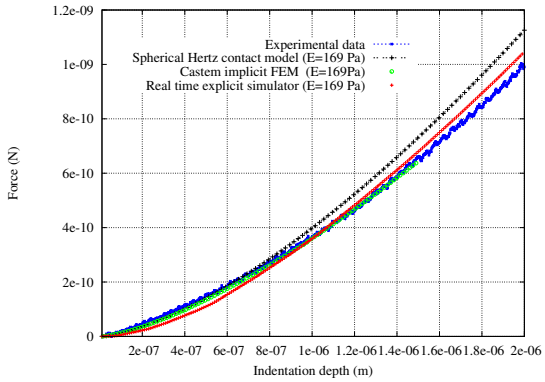

Fig. 9. Force versus indentation for live mESC: Comparison between the real-time FEM, the Hertz contact, the quasi-static FEM and experimental data .

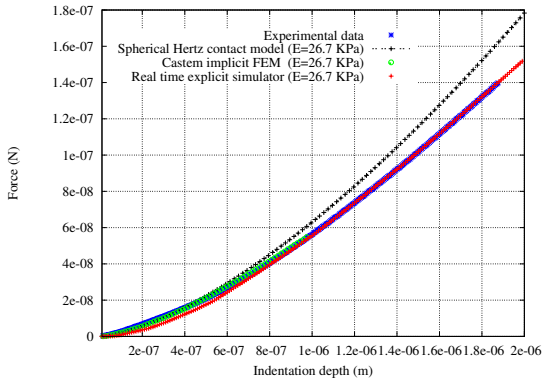

Fig. 10. Force versus indentation for fixed mESC: Comparison between the real-time FEM, the Hertz contact, the quasi-static FEM and experimental data .

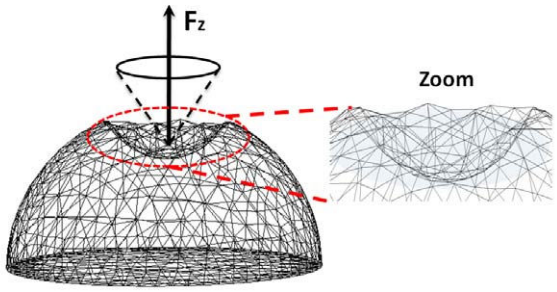

Fig. 11. Depth deformation of the cell; the left picture presents the depth indentation ($2\mu m$) of the cell, the right picture show the zoom of the cell deformation .

agreement with both Hertz contact model and experimental indentation data. In order to improve the force feedback rendering, we added a visual metaphor on the computer screen. The rendered reflection force is represented by a cone representing the force vector acting on the AFM tip. The visual metaphor has efficiently proved its effectiveness in AFM-based nanomanipulation simulation [18]. The vector amplitude reflects the force feedback amplitude and the vector orientation represents the vertical/horizontal force components. The fig.11 shows 3-D real-time probe tip, zoomed cell indentation, and microforces. The indentation force

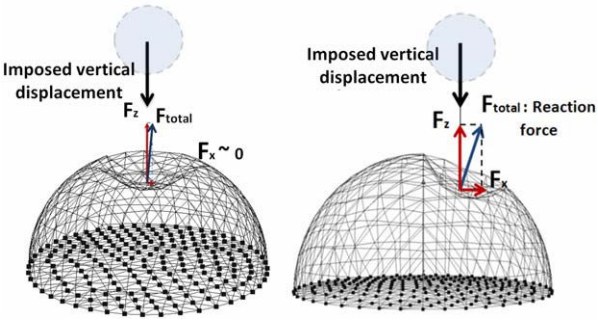

(a) (b)

Fig. 12. The force indentation where the probe is put without corresponding to the center of cell.

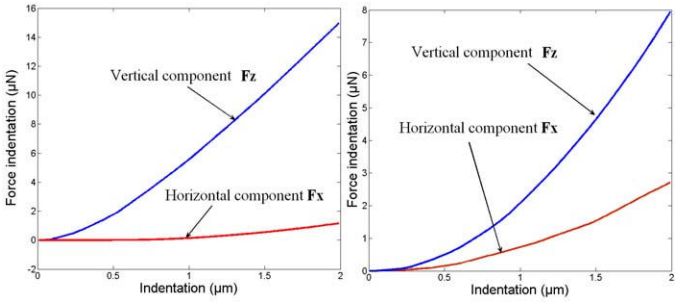

(a) (b)

Fig. 13. The horizontal and vertical component force versus indentation, (a); the probe is put in the center of the cell, (b); the probe is put without corresponding to the center of cell.

rendered to the operator is composed of a vertical F_z and horizontal F_x component. For the specific case corresponding to the center indentation, the tangential component is very small $F_x \simeq 0$. Only vertical reflection force is provided to the user. He cannot haptically feel it during simulated indentation tests (see fig.12.(a) and fig.13.(a)). In the case where the AFM probe is pushed away from the center of the cell, the tangential component exists $F_x \neq 0$ and the reflection force rendered to the user contains a vertical and tangential component (see fig.12.(b) and fig.13.(b)). We did not reproduce this specific case in our results since the main interest of the paper is to prove experimentally the real-time explicit simulator results during centered cell indentations.

VII. Conclusions

We have developed a computer-based training system to simulate real-time cell indentation procedures in virtual environments for training biologists residents. The simulator provides the user with visual and haptic feedback. The simulation of this procedure involves the real-time rendering of computer generated graphical images of AFM tip, physically-based modeling of soft biological tissue, and display of touch and force sensations to the training through the simulation of haptic interactions. We first investigated the challenging issues in the real-time modeling of the biomechanical properties of the cell indentation through finite element models. Compared to experimental AFM indentation results performed on mESC. Currently, we are working on integrating nanoscale effects such as friction, viscosity, punction. All modalities will be merged in an ergonomic tool and intelligent biological simulator for stem cell characterization.

References

[1] J. Settleman, *Tension precedes commitment-even for a stem cell. Mol Cell*, vol.14, pp. 148-150, 2004.

[2] J.Desai, A.Pillarisetti, A. D.Brooks ,*Engineering Approaches to Biomanipulation*, Annual Review of Biomedical Engineering, 9, pp. 35-53, 2007.

[3] F. Arai, D. Ando, T. Fukuda, Y. Nonoda, T. Oota, *Micromanipulation based on micro physics, strategy based on attractive force reduction and stress measurement*, in Proc. IEEE Int. Conf. Robotics Automation, pp. 236-241, 1995.

[4] Bausch AR, Moller W, and Sackmann E., *Measurement of local viscoelasticity and forces in living cells by magnetic tweezers*, Biophys Journal, vol.76, pp.573-579, 1999.

[5] T. Ohasti, M. Hagiwara, D. L. Bader, N. M. Knight, *Intracellular mechanics and mechanotransduction associated with chondrocyte deformation during pipette aspiration*, Biorheology, vol. 43, no3-4, pp. 201-214, 2006.

[6] J. L. Alonso and W. H. Goldmann, *Feeling the forces: atmoic force microscopy in cell biology*, Life Sciences, vol. 722553 - 2560, 2003.

[7] A. Touhami, B. Nysten, and Y. F. Dufrene, *Nanoscale mapping of the elasticity of microbial cells by atomic force microscopy*, Langmuir, vol. 19 pp 4539 - 4543, 2003.

[8] Darling, E.M., S. Zauscher, and F. Guilak, *Viscoelastic properties of zonal articular chondrocytes measured by atomic force microscopy*, Osteoarthritis Cartilage, 14:571-579, 2006.

[9] Mahaffy, R.E., S. Park, E. Gerde, J. Kas, and C.K. Shih. *Quantitative analysis of the viscoelastic properties of thin regions of fibroblasts using atomic force microscopy*, Biophys. J. 86:1777-1793, 2004.

[10] Alcaraz, J., L. Buscemi, M. Grabulosa, X. Trepat, B. Fabry, R. Farre, and D. Navajas, *Microrheology of human lung epithelial cells measured by atomic force microscopy*, Biophys. J. 84:2071-2079, 2004.

[11] A. Pillarisetti, C. Keefer, J. P. Desai, *Mechanical Response of embryonic stem cells using haptics-enabled atomic force microscopy*, in International Sympoisum on Experimental Robotics, Athens, Greece, 2008

[12] Valentin Lulevich, Tiffany Zink, Huan-Yuan Chen, Fu-Tong Liu, and Gang-yu Liu, *Cell Mechanics using Atomic Force Microscopy-based Single-Cell Compression*, Langmuir, vol. 22, no. 19, 2006, pp. 8151 - 8155.

[13] M. Bro-Nielsen and S. Cotin, *Real-Time Volumetric Deformable Models for Surgery Simulation Using Finite Elements and Condensation*, Computer Graphics Forum (Eurographics), vol. 5, no. 3, 1996, pp. 57-66.

[14] J.-M. Schwartz, M. Dellinger, D. Rancourt, C. Moisan, and D. Laurendeau, *Modeling Liver Tissue Properties Using a Non-linear Visco-Elastic Model for Surgery Simulation*, Medical Image Analysis, vol. 9, no. 2, 2005, pp. 103-112. 1.

[15] H.Ladjal, J-L.Hanus, A. Pillarisetti, C. Keefer, A.Ferreira and J. P. Desai , *Atomic Force Microscopy-Based Single-Cell Indentation: Experimentation and Finite Element Simulation*, IEEE International Conference on Robots and Intelligent Systems, October 11-15, 2009, Hyatt Regency St. Louis Riverfront, St. Louis, USA.

[16] A. Pillarisetti, H.Ladjal, C. Keefer, A.Ferreira and J. P. Desai *Mechanical Characterization of Mouse Embryonic Stem Cells*, in 31st Annual International IEEE EMBS Conference, September, 2-6, 2009, Hilton Minneapolis, Minnesota, USA

[17] A. Pillarisetti, C. Keefer, J. P. Desai, *Mechanical Response of embryonic stem cells using haptics-enabled atomic force microscopy*, in International Sympoisum on Experimental Robotics, Athens, Greece, 2008.

[18] W. Vogl, K-L-Ma. Bernice, M. Sitti, *Augmented reality user interface for an atomic force microscope-based nanorobotic system*, IEEE transactions on nanotechnology, 5(4), 397-406, 2006

[19] R. Adams, M. Moreyra, B. Hannaford , *Stability and performance of haptic displays : theory and experiments*, Proceedings of the ASME Winter Annual Meeting Haptics Workshop, Anaheim, USA, 1998.